Utrecht University

THE OCEAN CLEANUP

Investigating the role of submesoscale eddies for the accumulation of floating plastic debris in the eastern North Pacific Ocean

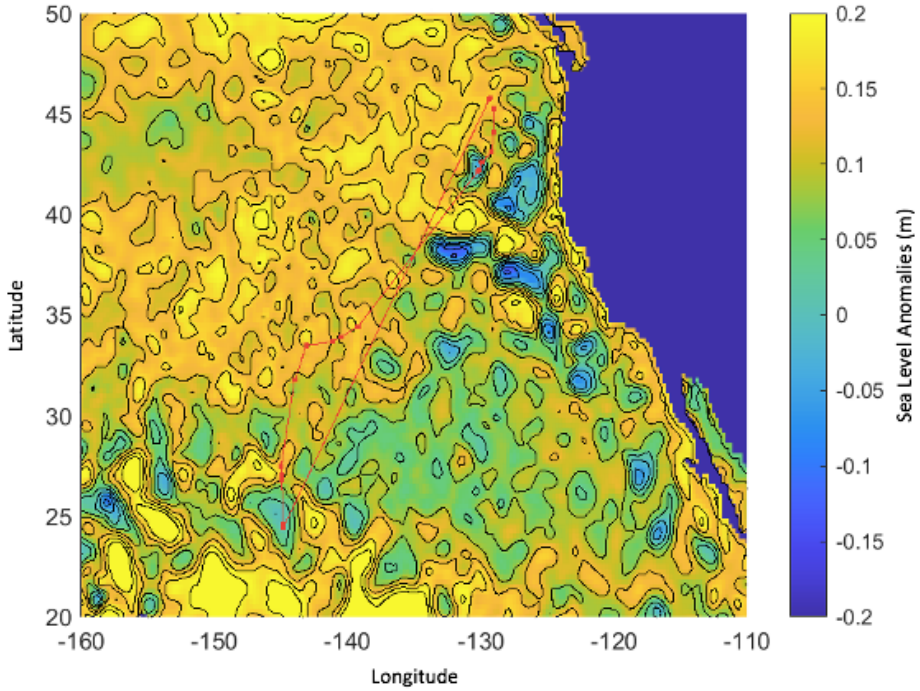

Lauren Quiros
Student No: 6374891
l.d.quiros@students.uu.nl
atpldquiros@gmail.com
Supervisor: Dr. Matthias Egger
Supervisor: Dr. Thilo Behrends
August 24th, 2020
Master Thesis (GEO4-1520)
Marine Sciences Master's Program

Abstract

Buoyant plastic debris is an increasing source of pollution threatening marine environments. As floating plastic debris moves from the shore to the open ocean, they are found to accumulate in large-scale converging circulation patterns called subtropical gyres or garbage patches. Previous in-situ observations give insight into the spatial heterogeneity distribution of floating marine debris at the ocean surface. However, minimal research has yet to take into account how submesoscale eddies, ocean circulation patterns described as 1-100 km diameter vorticities, can influence the accumulation and transport of floating plastic debris at the sea surface. Traditionally, there are two types of submesoscale eddies, cyclonic (a counterclockwise low pressure rotational dispersal system) and anti-cyclonic (a clockwise high pressure rotational accumulation system). The aim of this study is to investigate how the abundance, weight, characteristics, and variability of buoyant plastic debris is influenced by cyclonic and anti-cyclonic submesoscale eddies analyzed from three different regions in relation to the Great Pacific Garbage Patch (GPGP). Using daily satellite observations to identify anti-cyclonic and cyclonic submesoscale formations, floating plastic debris was extracted from the sea surface outside the GPGP, in the transition zone into the GPGP, and inside the GPGP. Due to the anti-cyclonic accumulating rotational dynamic, it is hypothesized that anti-cyclonic submesoscale eddies will accumulate a higher concentration of floating plastic debris in comparison to cyclonic submesoscale eddies. The results demonstrate a trend of cyclonic eddies accumulating higher concentrations than anti-cyclonic eddies within the outside and the transition zone into the GPGP. While anti-cyclonic eddies show a trend in accumulating higher concentrations of floating plastic debris inside the GPGP. Hard ('H') type plastics with the size range between 0.05 cm to 0.15 cm (Micro 1) was a common trend also found within the anti-cyclonic submesoscale measurements. While this study highlights how physical oceanic processes impact the dispersal of floating plastic debris, further research is required into plastic debris distribution patterns since these findings exhibited large spatial heterogeneity distribution of floating plastic debris found within submesoscale eddies.

Table of Contents

Abstract ____ ***2***

Table of Contents ____ ***3***

1. Introduction ____ ***4***

2. Methods ____ ***7***

2.1. Sampling ____ 7

2.2. Sample Processing ____ 9

2.3. Correction for wind-induced mixing ____ 11

2.4. SLA Data ____ 12

2.5. Dispersal Model ____ 12

3. Results ____ ***13***

3.1. Region A: Outside the Great Pacific Garbage Patch ____ 14

3.2. Region B: Transition Zone of the GPGP ____ 16

3.3. Region C: Inside the GPGP ____ 19

3.4. Spatial heterogeneity in plastic concentrations within and between sampling stations ____ 21

3.5. Measured vs. modelled plastic concentrations ____ 23

4. Discussion ____ ***24***

4.1. Spatial heterogeneity in floating plastic concentrations within and between sampling stations 24

4.2. Submesoscale eddies and Buoyant Plastic Debris Characterization ____ 24

4.3. Cyclonic Submesoscale Eddies within the Outer and Transition Zone into the GPGP ____ 25

4.4. Anti-cyclonic Submesoscale Eddies Inside the GPGP ____ 26

4.5. Limitations and Future Research ____ 27

4.6. Mitigation Strategies ____ 28

5. Conclusion ____ ***29***

6. References ____ ***30***

7. Acknowledgments ____ ***32***

1. Introduction

Marine plastic pollution often results in plastic contamination in various marine ecosystems, including coastlines, the oceanic surface, the water column, the deep sea, and the seabed (Law et al., 2017). These encounters can have negative impacts on the aquatic life in various ways such as entanglement, suffocation and starvation upon ingestion, discharging of toxic chemicals, and acting as a vehicle by dispersing invasive and potentially harmful species (UNEP, 2016). Presently, more than 65.5 % of plastics produced worldwide have a lower density than sea water (Geyer et al., 2017). As floating plastic debris transitions from shore into the open ocean, large-scale converging oceanic currents accumulate high concentrations of buoyant plastic particles which are more commonly referred to as gyres or garbage patches (Sigler, 2014).

The largest garbage patch is located between Hawaii and California, covering a span of 1.6 million km^2 in the eastern North Pacific Ocean, and has been coined the name, the Great Pacific Garbage Patch (GPGP) (Law et al., 2010; Goldstein et al., 2013; Van Sebille, 2015). However, estimates of only 250,000 metric tons are currently reported regarding the positively buoyant plastic debris afloat at sea, highlighting a major portion of missing floating plastic that should be in the tens of millions of metric tons atop the open ocean (Lebreton et al., 2019). Monitoring and assessing plastic debris and its long-term fate remains a challenge due to the large spatial and temporal heterogeneity in plastic concentration and accumulation areas along the sea surface within the GPGP (Ryan et al., 2009; Goldstein et al., 2013). In addition, concentrations of floating plastic debris at the sea surface collected in between sampling campaigns show large variability, occasionally an order of magnitude within only a few tens of kilometers (Lebreton et al., 2018). These examples highlight the limitations in our understanding of scales of spatial heterogeneity of floating plastic debris which could assist in understanding the whereabouts of the missing plastic. This is a critical knowledge gap needed to better assess and understand the impacts of plastic pollution on marine life within the eastern North Pacific Ocean. Therefore, knowing where and how buoyant plastic accumulates is essential for ecological risk assessments.

There are a variety of physical oceanic processes that influence the transport and accumulation of floating marine plastic debris. The most relevant oceanic processes that play a role in determining the trajectory and fate of the positively buoyant plastic objects within the open ocean are stokes drift, windage, Langmuir circulations, internal tides, submesoscale eddies, mesoscale eddies, and large-scale open ocean processes (Van Sebille et al., 2020). Stokes drift is the speed at which the floating particle moves due to wave propagation. Direct wind transport (windage) effects protruding buoyant plastic debris which are exposed at the sea surface. Langmuir circulations create convergence and divergence zones due to wind-induced shear flow and wave-induced stokes drift. Internal tides are generated due to the interaction between ocean floor bathymetry and barotropic (fluid density that only depends on pressure) tide. Mesoscale eddies are large, slow rotating vortices, 100s of km in diameter with a residency time between months to years. Submesoscale eddies are smaller and faster vortices, ranging from 1 to 100 km in diameter, with a residency time between days to weeks.

Advances in observational technology such as satellites have revealed how submesoscale eddies are key oceanic contributors which can trap and transport heat, nutrients, and other flotsam material (Chelton et al., 2011; Zhang et al., 2014; Van Sebille, 2015). There are two types of submesoscale eddies, cyclonic and anti-cyclonic eddies. Cyclonic eddies demonstrate an anti-clockwise (in the Northern Hemisphere), low pressure, upwelling rotation which tends to disperse flotsam material. While anti-cyclonic eddies are clockwise (in the Northern Hemisphere), high pressure, downwelling rotations which capture buoyant surface material (Cheng et al., 2014). Low and high Sea Level Anomalies (SLAs), taken from satellites, are proxies for determining cyclonic (low pressure) and anti-cyclonic (high pressure) eddies (Fu, 2010). To our knowledge, only one study investigated the submesoscale eddy impact regarding plastic debris distribution at the sea surface within the North Atlantic subtropical gyre. Their findings show concentrations of floating plastic debris was approximately 9.4 times higher in an anti-cyclonic submesoscale eddy in comparison to a cyclonic eddy (Bach et al, 2018). It is of interest to know whether a similar pattern of floating plastic accumulation can be observed in the eastern North Pacific Ocean.

Therefore, the aim here is to investigate the abundance, weight, characteristics, and variability of buoyant plastic debris between cyclonic (low pressure) and anti-cyclonic (high pressure) submesoscale eddies. Through this study, the following questions were asked; What is the floating plastic debris numerical concentration gradient between a cyclonic and anti-cyclonic submesoscale eddy? What is the floating plastic debris mass concentration gradient between a cyclonic and anti-cyclonic submesoscale eddy? What type and class size of floating plastic debris are found within cyclonic and anti-cyclonic submesoscale eddies? How does the floating plastic debris dispersal model compare to in-situ measurements corresponding to cyclonic and anti-cyclonic parameters?

2. Methods

2.1. Sampling

The Ocean Cleanup's North Pacific Mission 3 (NPM3) collected data from 45 neuston trawls that were deployed during a 32-day expedition (11th November -12th December 2019) on board the Maersk Transporter (MT) research vessel. Mesoscale ocean circulation patterns (vortices between 50 to 200 km in diameter) were identified by daily satellite measurements of Sea Level Anomalies (SLAs) and ocean current forecasts. The satellite data was coordinated and analyzed daily by the onshore research team of The Ocean Cleanup.

Furthermore, we divided our sampling sites into three regions in relation to the Great Pacific Garbage Patch (GPGP). Region A, B, and C correspond to outside GPGP, transition zone into the GPGP, and inside into the GPGP, respectively (Figure 1). Each location represents surface waters which have been identified with different concentrations of buoyant plastic debris (Lebreton et al., 2018). The samples in Region A (n=18) were collected in waters with modelled concentrations of floating debris of <10^4 #/km^2, Region B (n=12) between 10^4-10^5 #/km^2, and Region C (n=15) of >10^5 #/km^2.

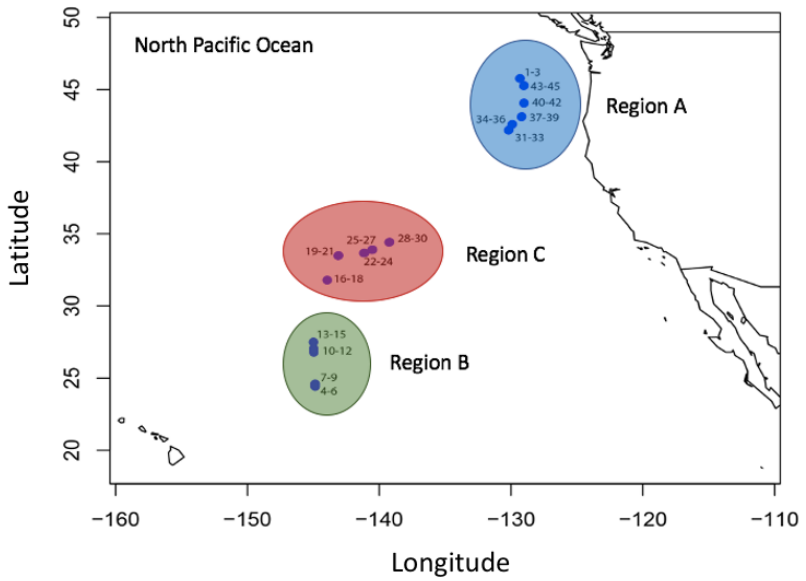

FIGURE 1| Map of North Pacific Ocean. The blue, red, and green circles mark Region A (outside GPGP), B (transition Zone), and C (inside GPGP), respectively. Individual samples (n = 45) represented by the dark blue points.

Each sampling station consist of 3 consecutive Manta trawl deployments which collected surface debris for 30 minutes at approximately 2 knots and covered approximately 2 km per trawl. The GPS coordinates were recorded at the beginning and end of each trawl completion. A Manta trawl (Ocean Instruments, Inc: mouth opening of 90 x 15 cm (width x height); 500 µm square mesh net) equipped with a flow meter (General Oceanics, Inc.) to measure the volume of filtered water was used throughout the sampling campaign. After each deployment trawl, the net was rinsed from the outside with fresh water and the cod-end (333 µm mesh size) removed, sealed with staples, placed in individually-labeled zip-lock bags, wrapped in aluminum foil, and stored frozen (-20 C°) for subsequent analysis of plastic particles in the onshore laboratory. Relevant metadata for all 45 trawl deployments such as dates, coordinates, and sea state per station are provided in Table 1.

TABLE 1| Metadata for North Pacific Mission 3 Expedition.

Station	Manta Trawl #	Date	Coordinates		Distance	Sea State	SLA*
		(UTC)	LAT	LON	km	Beaufort	m
1	Manta 001	22.11.2019	45.77	-129.31	0.959	3	0.185
	Manta 002	22.11.2019	45.78	-129.32	1.965	3	0.185
	Manta 003	22.11.2019	45.76	-129.34	1.911	3	0.186
2	Manta 004	28.11.2019	24.40	-144.86	1.583	2	-0.003
	Manta 005	28.11.2019	24.43	-144.86	1.338	2	-0.003
	Manta 006	28.11.2019	24.44	-144.86	1.715	2	-0.004
3	Manta 007	29.11.2019	24.57	-144.86	1.395	2	-0.006
	Manta 008	29.11.2019	24.59	-144.86	1.505	2	-0.006
	Manta 009	29.11.2019	24.60	-144.86	1.774	2	-0.007
4	Manta 010	29.11.2019	26.77	-144.96	1.942	3	0.130
	Manta 011	29.11.2019	26.92	-144.97	1.473	3	0.147
	Manta 012	29.11.2019	27.05	-144.97	2.021	3	0.160
5	Manta 013	29.11.2019	27.46	-144.99	1.796	4	0.172
	Manta 014	29.11.2019	27.48	-144.98	1.703	4	0.171
	Manta 015	29.11.2019	27.50	-144.98	1.735	4	0.170
6	Manta 016	2.12.2019	31.79	-143.98	2.419	5	0.103
	Manta 017	2.12.2019	31.78	-143.95	1.355	5	0.101
	Manta 018	2.12.2019	31.78	-143.93	2.048	5	0.101
7	Manta 019	3.12.2019	33.48	-143.12	1.831	4	0.157
	Manta 020	3.12.2019	33.48	-143.10	1.975	4	0.157
	Manta 021	3.12.2019	33.49	-143.07	1.918	4	0.158
8	Manta 022	3.12.2019	33.66	-141.17	1.644	4	0.105
	Manta 023	3.12.2019	33.66	-141.14	1.613	4	0.105
	Manta 024	3.12.2019	33.66	-141.11	2.004	4	0.103
9	Manta 025	3.12.2019	33.89	-140.55	2.155	4	0.118
	Manta 026	3.12.2019	33.89	-140.52	2.481	4	0.119
	Manta 027	3.12.2019	33.90	-140.49	2.037	4	0.119
10	Manta 028	4.12.2019	34.41	-139.26	1.867	2	0.165
	Manta 029	4.12.2019	34.42	-139.23	1.679	2	0.163
	Manta 030	4.12.2019	34.43	-139.20	1.891	2	0.161
11	Manta 031	7.12.2019	42.17	-130.18	1.910	4	-0.040
	Manta 032	7.12.2019	42.19	-130.17	1.968	4	-0.040
	Manta 033	7.12.2019	42.21	-130.15	2.114	4	-0.041
12	Manta 034	7.12.2019	42.57	-129.92	1.811	4	0.015
	Manta 035	7.12.2019	42.58	-129.91	1.780	4	0.020
	Manta 036	8.12.2019	42.60	-129.89	2.137	4	0.026
13	Manta 037	8.12.2019	43.09	-129.20	2.376	3	0.124
	Manta 038	8.12.2019	43.12	-129.19	2.040	3	0.123
	Manta 039	8.12.2019	43.14	-129.18	1.978	3	0.122
14	Manta 040	9.12.2019	44.04	-129.01	1.804	2	0.089
	Manta 041	9.12.2019	44.06	-129.01	1.673	2	0.090
	Manta 042	9.12.2019	44.08	-129.01	1.807	2	0.089
15	Manta 043	9.12.2019	45.29	-129.00	1.794	4	0.143
	Manta 044	9.12.2019	45.27	-129.01	1.897	4	0.143
	Manta 045	7.12.2019	45.25	-129.03	1.732	4	0.143

*Sea Level Anomaly (SLA)

2.2. Sample Processing

All 45 trawl samples were analyzed at The Ocean Cleanup laboratory located at the Rotterdam Zoo (Diergarde Blijdorp) in the Netherlands. The same procedure as described in Lebreton et al. (2018) and Egger et al. (2020) was applied to enable comparability with previous sampling investigations within the eastern North Pacific Ocean. The content of each cod-end was washed into a stainless-

steel tower sieve (5.0, 0.5, 0.15, 0.05 cm square apertures) which divided the plastic debris into the following size class: 0.05-0.15 cm (small microplastics; 'Micro1'); 0.15-0.5 cm (large microplastics; 'Micro2'); 0.5-1.5 cm (small mesoplastics; 'Meso1'), and 1.5-5 cm (large mesoplastics; 'Meso2') (Table2). Plastic objects >5 cm were excluded in this study due to an underestimation bias of fragments in this size class when sampling with neuston trawls (Lebreton et al., 2018). In order to extract the buoyant plastic from the sieves, each size class sieve was separately placed into round aluminum tins filled with North Atlantic Ocean seawater (filter: <1 µm; salinity: 35). The sieve content was manually stirred until all debris particles were detached from non-buoyant organic material.

TABLE 2 | Plastic Size Class (Lebreton et al., 2018)

Plastic Size Class	Abbreviation	Size Range
Small microplastics	Micro 1	0.05 – 0.15 cm
Large microplastics	Micro 2	0.15 – 0.5 cm
Small mesoplastics	Meso 1	0.5 – 1.5 cm
Large mesoplastics	Meso 2	1.5 – 5 cm

Subsequently, floating items identified as buoyant anthropogenic debris, described by Hidalgo-Ruz et al. (2012) were manually picked from the sieve using stainless-steel tweezers and their widest dimension was measured with a ruler. Each plastic particle was also quantitatively categorized by the following type of plastic (Lebreton et al., 2018; Egger et al., 2020): 'H-type' for fragments and objects made of hard plastic; 'N-type' for fragments of plastic lines, ropes, and fishing nets; 'P-type' for pre-production plastic pellets in the shape of a cylinder, disk or sphere; 'F-type' for fragments or objects made of foamed material (e.g. expanded polystyrene) (Table 3). The extracted plastic particles were rinsed with osmotic water to avoid weighing the salt from the seawater, dried for 3 hours and 45 mins at 60°C, and categorically photographed using the Panasonic DMC-FZ1000 camera and Microscope LEICAMZ95. Subsequently, each type and size class were transferred into pre-weighed sealable plastic bags and weighed using a scale OHAUS Explorer EX324M (0.0001 g readability).

TABLE 3 | Plastic Type (Lebreton et al., 2018)

Plastic Types	Abbreviation	Common Origins
Hard	H	Fragments made of hard plastic, plastic sheet, or film
Net	N	Fragments of plastic lines, ropes, and fishing nets
Pellet	P	Pre-production plastic pellets in the shape of a cylinder, disk, or sphere
Foam	F	Fragments made of foamed material

2.3. Correction for wind-induced mixing

Floating plastic debris at the sea surface has the potential to mix within the upper region of the water column due to wind and wave turbulence (Kukulka et al., 2012; Reisser et al., 2015). Therefore, to correctly estimate the vertical distribution of floating plastic objects, which could potentially be underestimated when deploying surface Manta trawls, a one-dimensional model (eq. 1) from Kukulka et al. (2012) was incorporated into the numerical concentrations (count of plastic per sea surface area). The floating plastic particles could be accounted for the upper 5 m of the water column when the equation is incorporated into the calculations. The towed area was calculated by multiplying the tow length (cataloged from the vessel GPS position data and flowmeter) and net mouth width.

$$C_i = \frac{C_s}{1-e^{-dW_b\left(1.5\sqrt{\frac{\rho_a}{\rho_w}C_d U^2}k\frac{0.96}{g}\sigma^{\frac{3}{2}}C_d U^2\right)^{-1}}} \qquad \text{(eq.1)}$$

C_s numerical concentration measured by the manta trawl (items per sea surface area)
d depth sampled by the manta trawl (in m)
W_b Terminal rising velocity of plastic (in m/s)
ρ_a air density (in kg/m^3)
ρ_w seawater density (in kg/m^3)
C_d drag coefficient
U wind speed during sampling (in m/s)
k Karman constant
g gravitational constant (in m/s)
σ wave age

In our case d equals 0.15 m, C_d equals 0.0012, k equals 0.4, g equals 9.81 m/s^2, and σ equals 35 (assuming a fully developed sea state). The depth-integrated concentrations were estimated using wind speeds equal to 0, 2, 5, 9, 13, and 19 knots for sampling campaigns corresponding with

Beaufort sea states 0, 1, 2, 3, 4, and 5, respectively. Lebreton et al. (2018) provided the median values for rising velocity measurements.

2.4. SLA Data

In order for the onboard research team to correctly extract surface samples from anti-cyclonic (high-pressure) and cyclonic (low-pressure) submesoscale eddies within the eastern North Pacific, the onshore research team measured daily Sea Level Anomalies (SLAs) from the Copernicus satellite online resource dataset.

2.5. Dispersal Model

The concentrations for various sizes and types of oceanic plastic can be approximated by multi-source and multi-forcing ocean plastic transport models. Here we use the model developed by Lebreton et al., (2018). The authors calibrated the numerical model using monthly averages of predicted concentrations that reflected seasonal and inter-annual changes within and around the Great Pacific Garbage Patch (GPGP). Particles were identically and continuously released in time from 1993 to 2012 following spatial distributions and amplitudes of significant ocean plastic sources on land (coastal population hotspots and major rivers) as well as at sea (fishing, aquaculture, and shipping industries). Advected global particles were influenced by the following environmental drivers: sea surface currents, wave induced stokes drift, and winds. The model predicted that micro- and mesoplastics accounted for 94% of the estimated 1.8 trillion plastic pieces floating within the GPGP.

3. Results

This study examined the abundance, weight, type, size and spatial distribution of marine plastic particles in correlation with Sea Level Anomalies (SLAs) obtained from satellite data. The three investigated regions are located in the eastern North Pacific Ocean, where Region A is located outside the Great Pacific Garbage Patch (GPGP), Region B is located in the transition zone of the GPGP and Region C lies inside the GPGP. The in-situ measurements taken at these three locations were compared to the plastic concentrations predicted for these regions by the ocean transport model from Lebreton et al. (2018). The SLAs were categorized into low, medium and high, which range from -0.041 m to 0.035 m, from 0.035 m to 0.110 m and from 0.110 m to 0.186 m, respectively.

The map in Figure 2 shows the geographical locations of regions A, B and C (black circles), as well as the trajectory of the research vessel (red line) along which the samples were taken. This map also reveals the wide array of sub mesoscale eddies circulating in the eastern North Pacific Ocean. The brighter colors depict regions with anti-cyclonic vorticities i.e. high SLAs whereas the darker colors represent regions of cyclonic vorticities i.e. lower SLAs. Our findings indicate that in general, the count (#/km^2) and mass (kg/km^2) plastic concentrations increase when moving from the outside towards the inside of the GPGP, i.e. when moving from region A to B to C (see table in Figure 2). The next three subsections will present the results for each of the three individual regions.

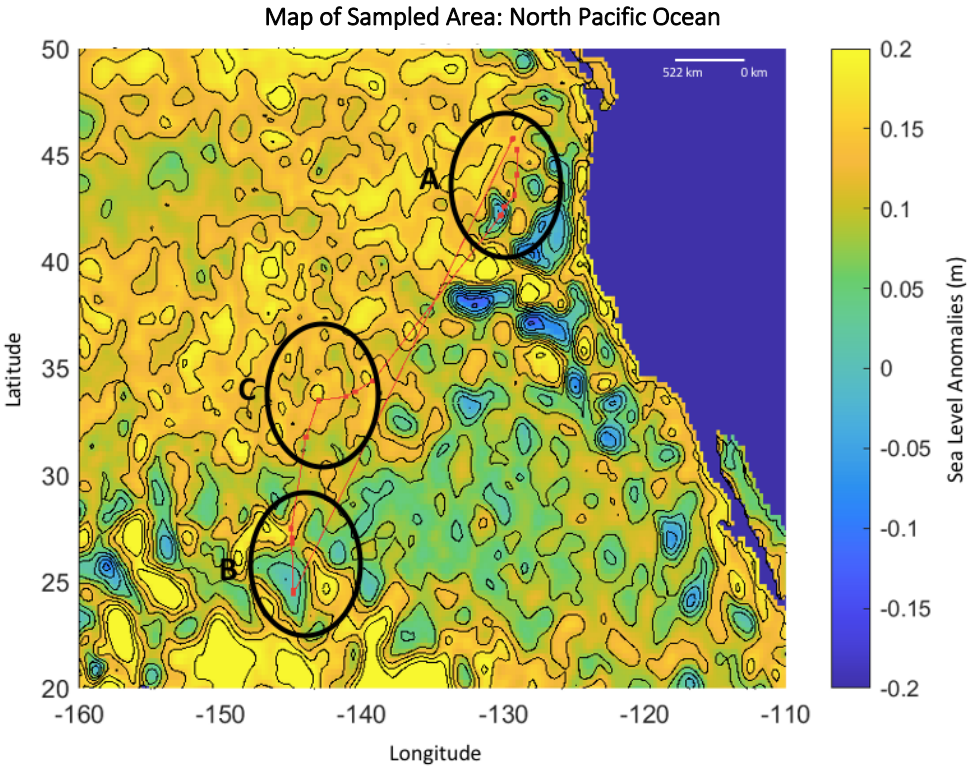

Region	Location *	Abundance (#/km²)	Weight (kg/km²)
A	Outside GPGP	15,047	0.023
B	Transition Zone GPGP	273,701	0.414
C	Inside GPGP	573,385	3.463

*Great Pacific Garbage Patch (GPGP)

Figure 2 | A map of the sampled area within the eastern North Pacific Ocean correlated with Sea Level Anomalies (SLAs) satellite observations obtained from the Copernicus monitoring service (on the 9th of December 2019). The boat track is shown as a red line and was obtained by coordinates; sampling sites locations are marked as red dots. The table describes the region, location name, median numerical concentration (#/km^2) and median mass concentration (kg/km^2) for floating plastic debris.

3.1. Region A: Outside the Great Pacific Garbage Patch

Figure 3 shows a table (3A) and a map (3B) depicting the measured floating plastic debris count concentrations measured in Region A, along with the corresponding SLA values in that area. The red dots in the map indicate the six sampling stations (i.e. manta trawl deployments) within this region of which the median plastic concentrations (#/km^2) are given in the table left of the map (Figure 3). The plastic concentrations found in the samples taken at locations 4, 5 and 6, demonstrate that when going from a high to low SLA, the number of floating plastic particles per

km^2 increases from 5,195 to 28,665 to 44,791. The highest concentration of 44,791 #/km^2 (sample station 6), was found in a cyclonic eddy with an SLA around -0.040 m.

Spatial Distribution of Floating Plastic Collected within Region A: Outside GPGP

A

Visualization	Median	SLA
#	#/km^2	m
1	28,985	0.185
2	13,625	0.143
3	3,322	0.089
4	5,196	0.123
5	28,665	0.020
6	44,791	-0.040

B

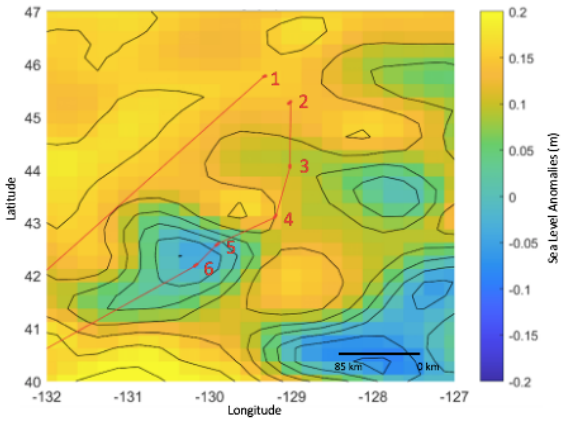

FIGURE 3 | Spatial distribution and accumulation (#/km^2) of floating plastic according to sea level anomaly (SLA) for Region A (outside GPGP). (A) Table regarding visualization number, median numerical concentration (#/km^2), and sea level anomaly (SLA) in m. (B) Map of the sampled area correlated with the SLA observations obtained from the Copernicus monitoring service (9th of December 2019) for Region A. The boat track is shown as a red line and was obtained by coordinates, each bolded red dot represents the approximate location of three Manta trawl deployments. Red numbers correlate to visualization number in table in A. Satellite data identified low pressure areas in purple and high pressure areas in yellow.

Figure 4A shows that the low SLA category contains the highest median plastic particle abundance concentration, namely 26,160 #/km^2, in comparison to the medium (3,321 #/km^2) and high (13,625 #/km2) SLA category. In addition, the range in plastic item density is highest in the low SLA category, namely 50,941 #/km^2, and 30,574 #/km^2 for the high SLA category. While the medium SLA range is much smaller at 4,919 #/km^2. Our findings demonstrate that for both the low and the high SLA categories, plastics of type H (low SLA: 70%; high SLA: 91%) and plastics of the size class Micro 1 (low SLA: 56%; high SLA: 59%) make up the largest fraction of the plastic assemblage. Figure 4B shows that the median plastic mass concentrations in the low, medium, and high SLA categories are similar, namely 0.022, 0.021, and 0.024 kg/km^2 respectively. However, the range of measured mass concentrations differ, as the low SLA category shows a range of 0.183 kg/km^2 and the high SLA category a range of 0.07 kg/km^2. In addition, our findings show that in both the low and the high SLA categories plastics of type H (low SLA: 63%; high SLA: 73%) make up the largest fraction in mass. In the low SLA category plastics of size class Micro 2 make up the largest fraction

(73%), whereas in the high SLA category plastics of size class Micro 1 make up the largest mass fraction (51%).

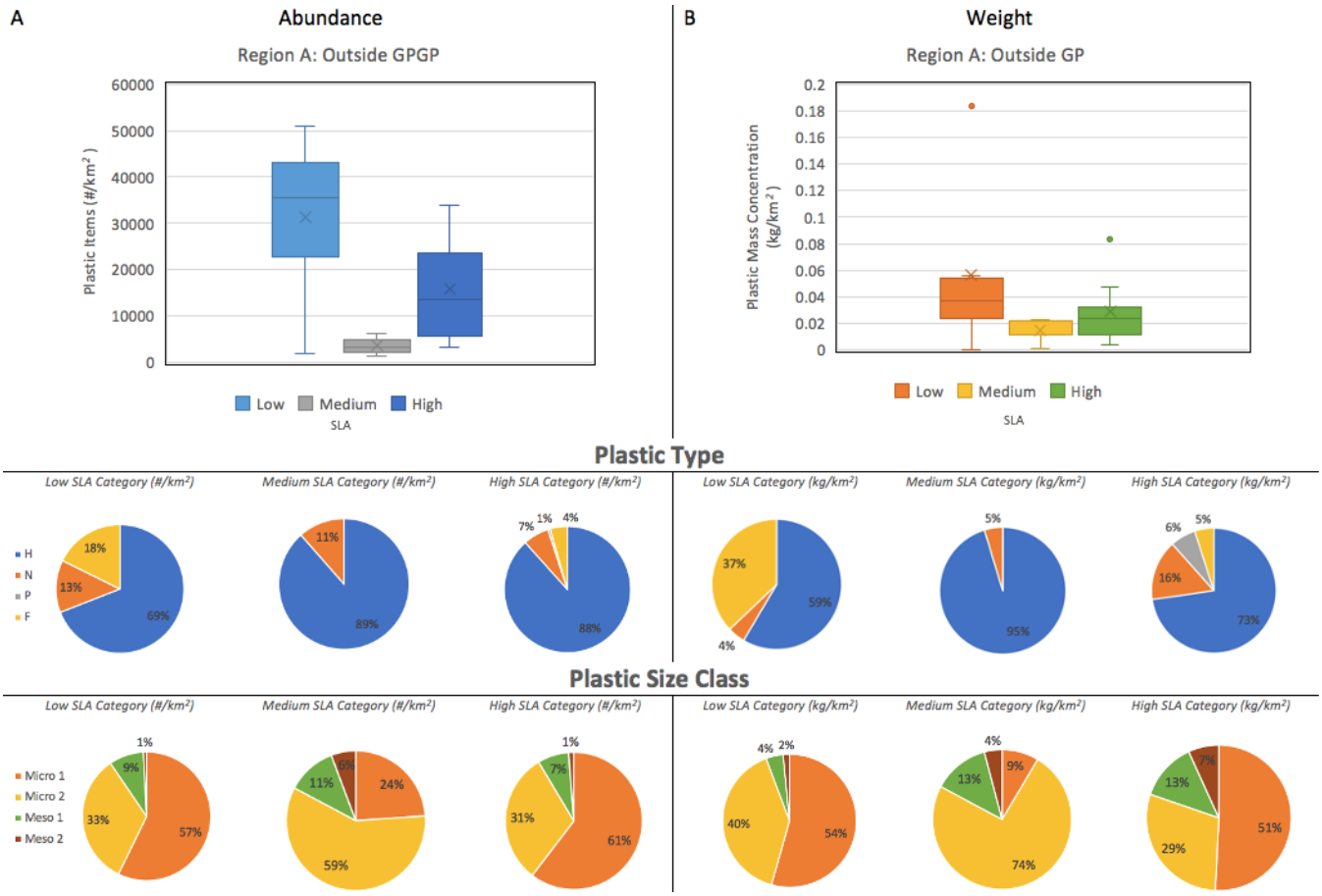

FIGURE 4 | Region A (outside GPGP) buoyant plastic items (#/km²), mass concentration (kg/km²), and characterization according to sea level anomaly categories (SLA, m): Low (-0.041 to 0.035 m); *Medium (0.036 to 0.110 m); and High (0.111 to 0.186 m). **(A)** Buoyant plastic items analyzed in numerical concentration (#/km²) **(B)** Buoyant plastic analyzed in mass concentration (kg/km²)**;** Median numerical concentrations are represented in bold line, mean numerical concentrations are marked by an x, boxes range from 25th to 75th percentiles and whiskers extend from minimum to maximum values not considering outliers which are plotted as dots and included in calculations (inclusive median boxplot calculations). **Types of Plastic**: 'H-type' for hard plastic; 'N-type' for plastic lines, ropes, and fishing nets; 'P-type' for pre-production plastic pellets; 'F-type' for foam material. **Plastic Class Size**: 'Micro1' (0.05-0.15 cm); 'Micro2' (0.15-0.5 cm); 'Meso1' (0.5-1.5 cm), and 'Meso2' (1.5-5 cm). *No samples taken within medium SLA range.

3.2. Region B: Transition Zone of the GPGP

Figure 5 shows a table (5A) and a map (5B) depicting the measured floating plastic debris count concentrations measured in Region B, along with the corresponding SLA values in that area. In Region B no samples were taken in the medium SLA category. The red dots in the map indicate the six sampling stations (i.e. manta trawl deployments) within this region of which the median

plastic concentrations (#/km^2) are given in the table left of the map (Figure 5). The SLA distribution reveals an anti-cyclonic submesoscale eddy located around 27.5^{o}N latitude and -145^o longitude, and a cyclonic submesoscale eddy around 24.5^{o}N latitude and -144.8^o longitude. The plastic concentrations found in the epicentre (sample station 7) of the anti-cyclonic eddy is 224,127 #/km^2, whereas this concentration is about three times higher in the epicentre (sample station 11) of the cyclonic eddy, i.e. 714,216 #/km^2. Moreover, there is a large spatial variation in plastic item concentration as sample station 12, which is only 50 km away from sample station 11, has a plastic item concentration 12 times smaller plastic item concentration, namely only 57,577 items per km^2.

Spatial Distribution of Floating Plastic Collected within Region B: Transition Zone into the GPGP

A

Visualization	Median	SLA
#	#/km^2	m
7	224,127	0.164
8	326,764	0.130
9	323,256	0.147
10	470,330	0.160
11	714,216	-0.006
12	57,577	-0.003

B

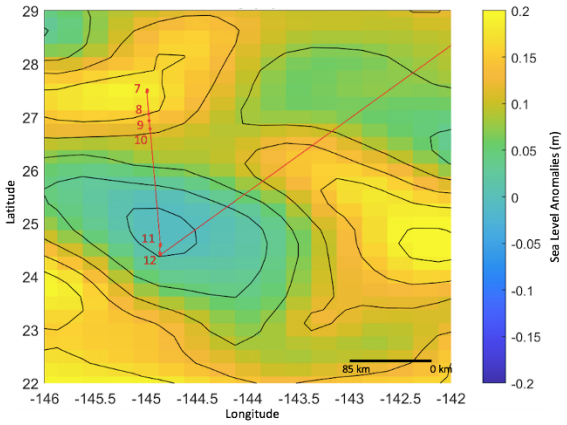

FIGURE 5 | Spatial distribution and accumulation (#/km^2) of floating plastic according to sea level anomaly (SLA) for Region B (transition zone of GPGP). (A) Table regarding visualization number, median (#/km^2), and sea level anomaly (SLA) in m. (B) Map of the sampled area correlated with the SLA observations obtained from the Copernicus monitoring service (29th of December 2019) for Region B. The boat track is shown as a red line and was obtained by coordinates, each bolded red dot represents the approximate location of three Manta trawl deployments. Red numbers correlate to visualization number in table in A. Satellite data identified low pressure areas (cyclonic vortices) in blue and high pressure areas (anti-cyclonic vortices) in yellow.

Figure 6A shows that the high SLA category contains the highest median plastic particle abundance concentration, namely 325,010 #/km^2, and the low SLA category shows a median plastic particle abundance concentration of 74,110 #/km^2. In addition, the range in plastic item density is approximately 2.4 times higher in the low SLA category (854,870 #/km^2) compared to the high SLA category (352,353 #/km^2). For both the low and the high SLA categories, plastics of type H (low SLA: 98%; high SLA: 95%) make up the largest fraction of the plastic assemblage. In the low SLA category plastics of size class Micro 2 make up the largest fraction (53%), whereas in the high SLA

category plastics of size class Micro 1 make up the largest fraction (56%). Figure 6B shows that the median plastic mass concentrations in the low SLA category, i.e. 0.205 kg/km^2 is 4.1 times smaller than in the high SLA category, i.e. 0.858 kg/km^2. The low SLA category shows a range of 3.311 kg/km^2 and the high SLA category a range of 1.874 kg/km^2. In both the low and the high SLA categories plastics of type H (low SLA: 94%; high SLA: 91%) make up the largest fraction in mass. In the low SLA category plastics of the size classes Micro 1 (36%), Micro 2 (27%) and Meso 1 (33%) together make up the largest mass fraction (96%), whereas in the high SLA category the plastics of size classes Micro 2 (47%) and Meso 2 (35%) together make up the largest mass fraction (82%).

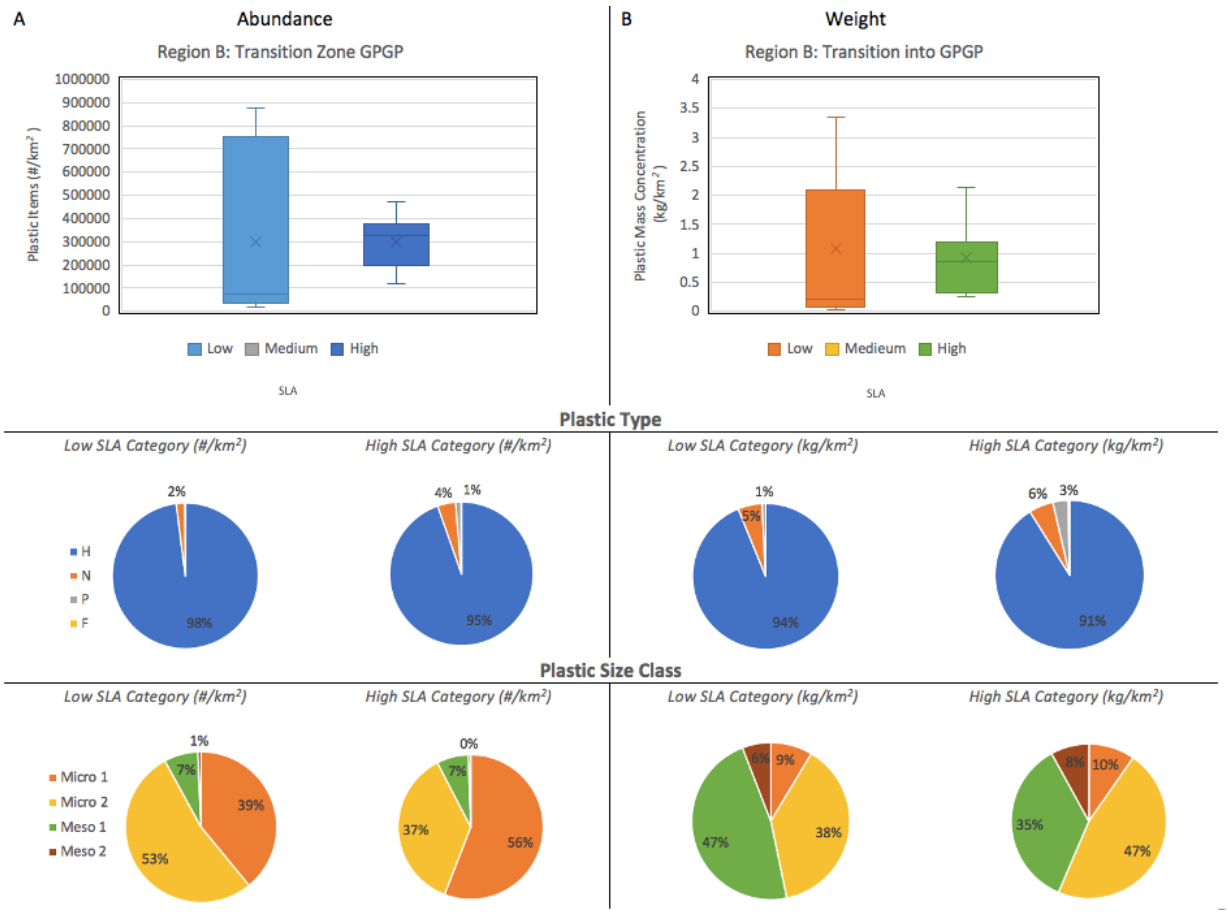

FIGURE 6 | Region B (transition zone GPGP) buoyant plastic items (#/km^2), mass concentration (kg/km^2), and characterization according to sea level anomaly categories (SLA, m): Low (-0.041 to 0.035 m); *Medium (0.036 to 0.110 m); and High (0.111 to 0.186 m). (A) Buoyant plastic items analyzed in numerical concentration (#/km^2) **(B)** Buoyant plastic items analyzed in mass concentration (kg/km^2)**;** Median numerical concentrations are represented in bold line, mean numerical concentrations are marked by an x, boxes range from 25th to 75th percentiles and whiskers extend from minimum to maximum values not considering outliers which are plotted as dots and included in calculations (inclusive median boxplot calculations). **Types of Plastic**: 'H-type' for hard plastic; 'N-type' for plastic lines, ropes, and fishing nets; 'P-type' for pre-production plastic pellets; 'F-type' for foam material. **Plastic Class Size**:

'Micro1' (0.05-0.15 cm); 'Micro2' (0.15-0.5 cm); 'Meso1' (0.5-1.5 cm), and 'Meso2' (1.5-5 cm). *No samples taken within medium SLA range.

3.3. Region C: Inside the GPGP

Figure 7 shows a table (7A) and a map (7B) depicting the measured floating plastic debris count concentrations measured in Region C, along with the corresponding SLA values in that area. In Region C no samples were taken in the low SLA category. The red dots in the map indicate the five sampling stations (i.e. manta trawl deployments) within this region of which the median plastic concentrations (#/km^2) are given in the table left of the map (Figure 7). The SLA distribution reveals several anti-cyclonic submesoscale eddies in Region C, of which only samples were taken from the one located around 34.5^{o}N latitude and -139^o longitude, and a second one located around 33.5^{o}N latitude and -143^o longitude. The median plastic concentrations found in the epicentre of the eastern anti-cyclonic eddy (sample station 13) is 1,257,553 #/km^2, and in the epicentre of the western anti-cyclonic eddy (sample station 16) a plastic concentration of 260,203 #/km^2 was found. Going from sample station 13 to 14 to 15, i.e. moving from higher to lower SLAs, the number of floating plastic particles per km^2 decreases from 1,257,553 to 564,919 to 496,887.

Spatial Distribution of Floating Plastic Collected within Region C: Inside GPGP

A

Visualization	Median	SLA
#	#/km^2	m
13	1,257,553	0.163
14	564,919	0.121
15	496,887	0.104
16	260,203	0.152
17	773,114	0.102

B

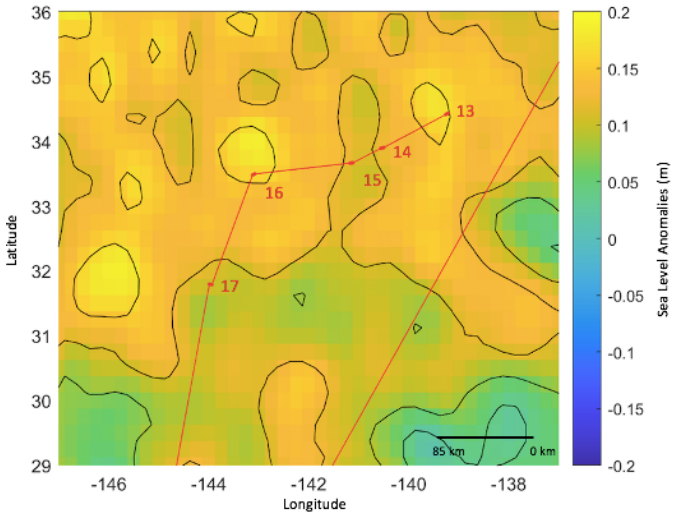

FIGURE 7 | Spatial distribution and accumulation (#/km^2) of floating plastic according to sea level anomaly (SLA) for Region C (inside GPGP). (A) Table of metadata regarding visualization number, sample ID, Date (coordinated universal time), coordinates (Latitude and Longitude), median (#/km^2), sea level anomaly (SLA) in m. (B) Map of the sampled area correlated with the average SLA observations obtained from the Copernicus monitoring service (4th of December 2019) for Region C. Each bolded X represents the approximate location of 3 Manta trawl deployments. Red numbers

correlate to visualization number on table in A. Black numbers correlate to median numerical concentration per X. Satellite data identified low pressure areas in blue and high pressure areas in yellow.

Figure 8A shows that the median plastic particle abundance concentrations in the medium and high SLA categories are similar, namely 575,487 and 573,385 #/km^2 respectively. However, the range in plastic item density are significantly different. In the medium SLA category this range is 1,040,690 #/km^2, while in the high SLA category the range is 3,356,864 #/km^2. For both the medium and the high SLA categories, plastics of type H (medium SLA: 80%; high SLA: 95%) make up the largest fraction of the plastic assemblage. In the medium SLA category plastics of size class Micro 1 make up the largest fraction (60%), whereas in the high SLA category plastics of size classes Micro 1 (49%) and Micro 2 (45%) together make up the largest fraction. Figure 8B shows that the median plastic mass concentrations in the medium SLA category equals 4.29 kg/km^2 and in the high SLA category it is 3.39 kg/km^2. The medium SLA category shows a range of 6.36 kg/km^2 and the high SLA category a range of 22.30 kg/km^2. In both the medium and the high SLA categories plastics of type H (medium SLA: 94%; high SLA: 91%) make up the largest fraction in mass. In the medium SLA category plastics of the size classes Micro 2 (40%), Meso 1 (33%) and Meso 2 (24%) together make up the largest mass fraction (97%), whereas in the high SLA category the plastics of size classes Meso 1 (33%), Meso 2 (32%) and Micro 2(29%) together make up the largest mass fraction (94%).

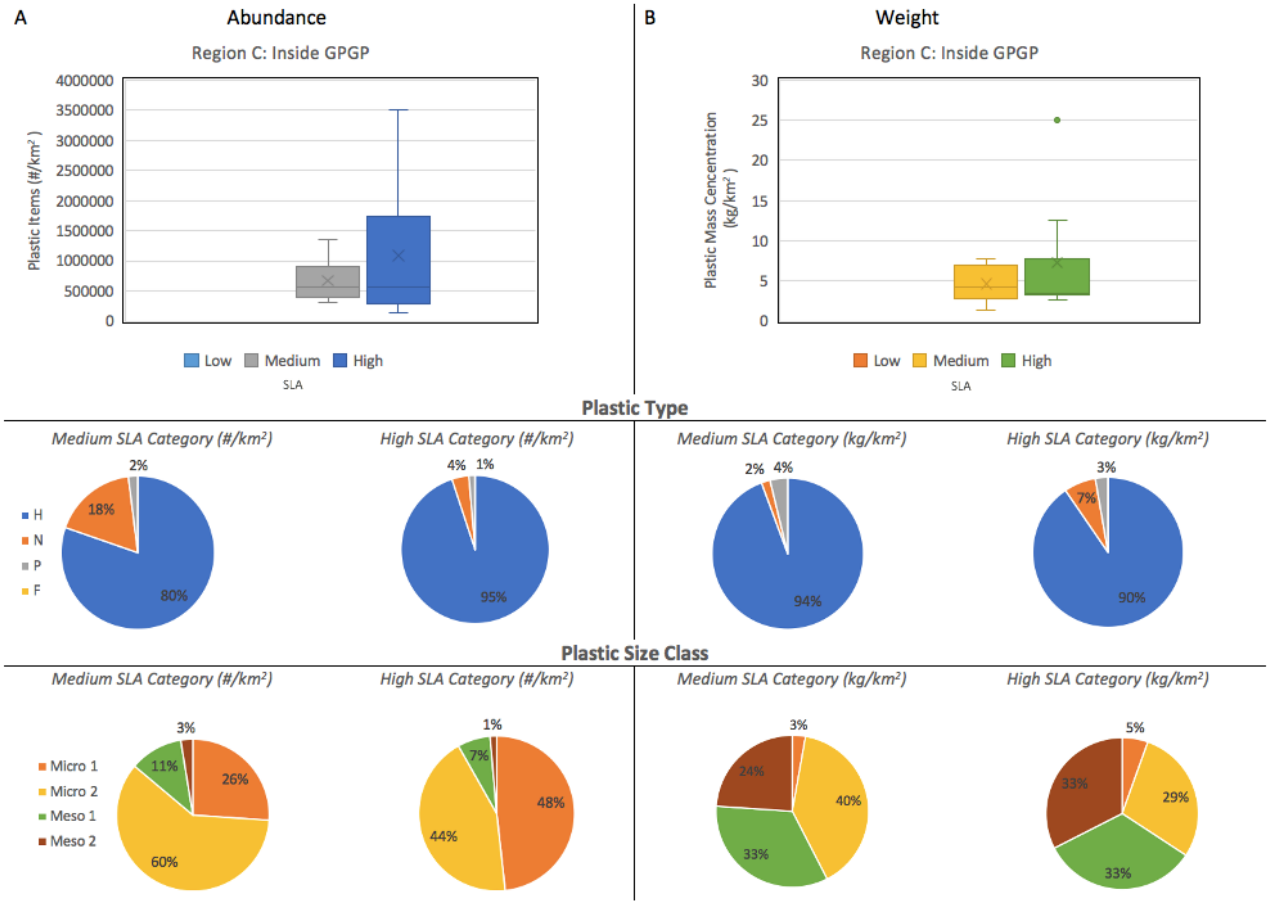

FIGURE 8 | Region C (inside GPGP) buoyant plastic items (#/km^2), mass concentration (kg/km^2), and characterization according to sea level anomaly categories (SLA, m): Low (-0.041 to 0.035 m); *Medium (0.036 to 0.110 m); and High (0.111 to 0.186 m). (A) Buoyant plastic items analyzed in numerical concentration (#/km^2) **(B)** Buoyant plastic items analyzed in mass concentration (kg/km^2)**;** Median numerical concentrations are represented in bold line, mean numerical concentrations are marked by an x, boxes range from 25th to 75th percentiles and whiskers extend from minimum to maximum values not considering outliers which are plotted as dots and included in calculations (inclusive median boxplot calculations). **Types of Plastic**: 'H-type' for hard plastic; 'N-type' for plastic lines, ropes, and fishing nets; 'P-type' for pre-production plastic pellets; 'F-type' for foam. **Plastic Class Size**: 'Micro1' (0.05-0.15 cm); 'Micro2' (0.15-0.5 cm); 'Meso1' (0.5-1.5 cm), and 'Meso2' (1.5-5 cm). *No samples taken within low SLA range.

3.4. Spatial heterogeneity in plastic concentrations within and between sampling stations

Figure 9 shows for all three regions (A, B and C) the variation in measured plastic particle abundance (^{10}log(#/km^2)) (9A) and mass (kg/km^2) (9B) concentrations for all sampling stations. The sampling stations on the horizontal axes of the box plots in Figure 9 are arranged according to their (average) SLA value in ascending order. The six sampling stations in Region A show two orders of magnitude variation in the plastic particle abundance concentrations, while in Region C the variation between the sampling stations was only one order of magnitude in particle abundance

(Figure 9A). Our findings show a variation of plastic concentrations within sampling station as well, for example sampling station 3 (Region A) and 7 (Region B) both show a range from of two orders of magnitude in particle abundance (Figure 9A). In Figure 9B, sampling station 1 (Region A), 7 (Region (B) and 13 (Region C) show plastic mass concentration range of 0.160, 3.311 and 21.516 kg/km^2, respectively (Figure 9B). In addition, the results indicate a general trend in numerical concentration (top panel: A) to decrease in regards to variation as the samples were taken from the outside moving inside of the GPGP. However, the opposite is occurring within the bottom panel (Figure 9B) as the variation between sampling campaigns is increasing within the mass concentrations recorded.

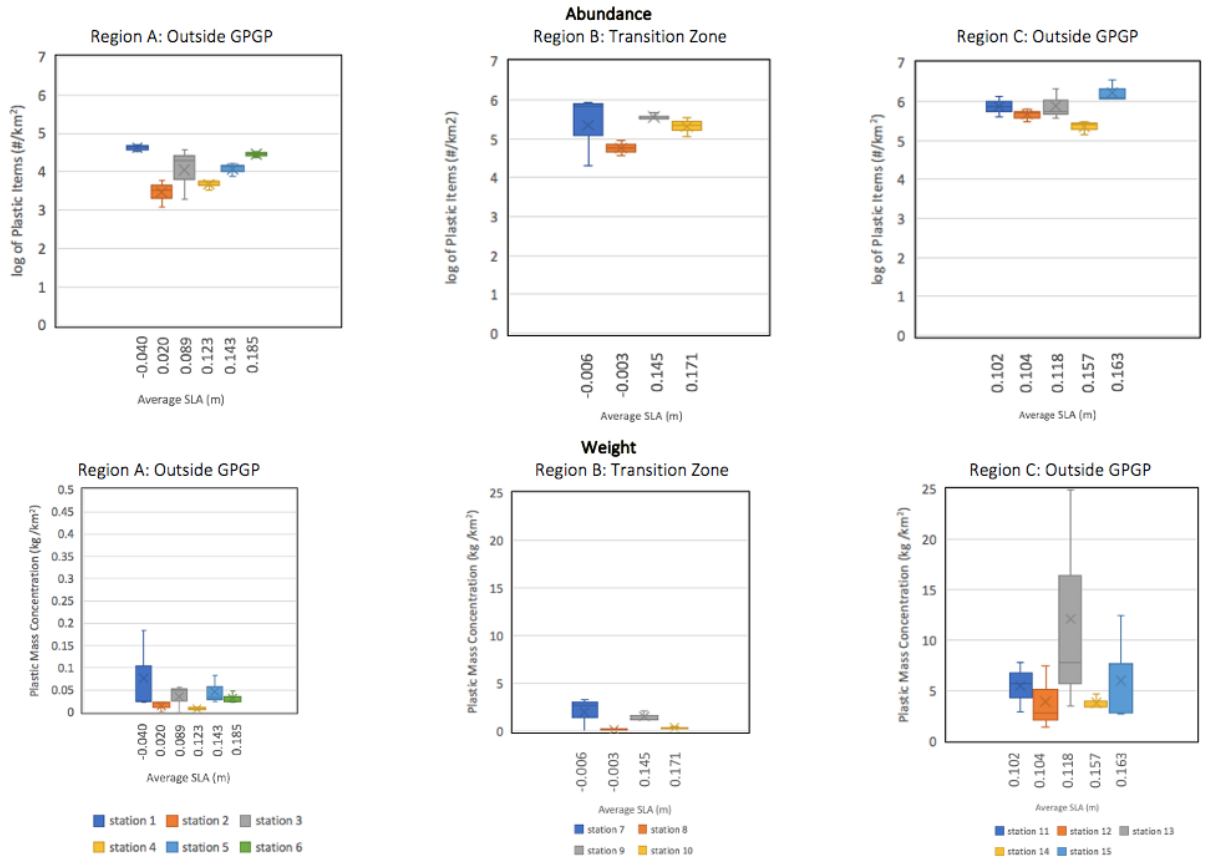

FIGURE 9 | Variation in buoyant plastic (A) items log(#/km^2) and (B) mass concentration (kg/km^2) per sampling station (one station = three Manta trawl deployment) for Region A (outside GPGP), B (transition zone GPGP), and C (inside GPGP). Median numerical concentrations are represented in bold line, mean numerical concentrations are marked by an x, boxes range from 25th to 75th percentiles and whiskers extend from minimum to maximum.

3.5. Measured vs. modelled plastic concentrations

Figure 10 shows our measured plastic particle abundance concentrations (y-axis) for the three regions (A, B and C) and the predicted plastic particle abundance concentrations (x-axis) from the oceanic transport model from Lebreton et al. (2018). This plot shows that the plastic particle abundance concentrations modelled for Region A (outside the GPGP) and B (transition zone) are underestimated by one to two orders of magnitude. For Region C, inside the GPGP, the plastic particle abundance concentrations are overestimated by the model by approximately one order of magnitude, according to our measured concentrations. The results show that the low SLA (marked as Xs) is more sporadically distributed (approximately between one to two order of magnitude for region A and B), while the medium and high SLA category is distributed more conservatively for region C by approximately one order of magnitude below the predicted model concentrations.

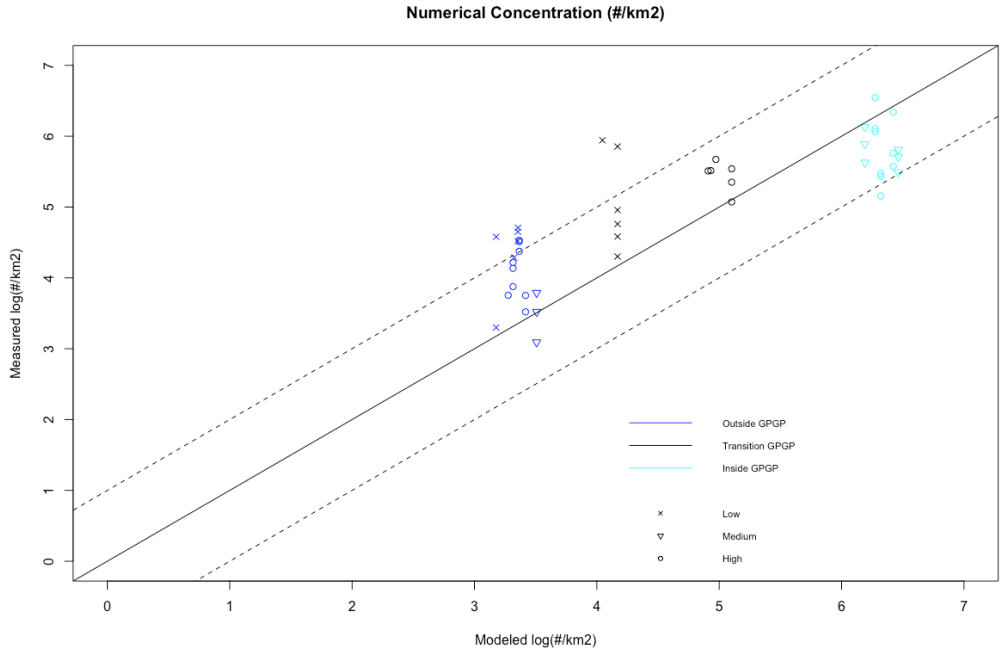

FIGURE 10 | Measured versus modeled of #/km2 of buoyant marine plastic in the North Pacific Ocean. Log scale indicates the measured versus modeled values (log(#/km^2)). The solid line is the 1 to 1 and the dotted line is an order of magnitude difference from the predicted concentration from the model. The blue, black, and aqua colors mark regions A, C, and B respectively. The x, triangle, and circle symbol represent low, medium, and high Sea Level Anomalies (SLA)s.

4. Discussion

4.1. Spatial heterogeneity in floating plastic concentrations within and between sampling stations

The results demonstrate large spatial heterogeneity in floating plastic debris concentrations within and between sampling stations (Figure 9A). Small-scale physical oceanic processes and location can play a role in influencing the variation in plastic accumulation concentrations. Langmuir circulations and internal tides are two oceanic processes that demonstrate convergencies of flotsam material with a bandwidth ranging between two to three meters (Van Sebille et al., 2020). Therefore, these high concentration bands of floating plastic debris can potentially be extracted throughout the sampling campaigns, further influencing the distribution. In addition, the general trend observed in Figure 9A shows high variations between and within Manta trawl deployments decreasing as the samples were taken from the outside of the Great Pacific Garbage Patch (GPGP) towards the inside of the GPGP. This decrease in heterogeneity may be due to the location. The GPGP is located farther away from major land masses, major currents, and internal tides. Therefore, this can contribute to a more homogenous distribution of floating plastic debris. However, it is important to keep the other ubiquitous physical oceanic processes into account, stokes drift and Langmuir circulations, that can potentially influence the spatial heterogeneity when taking samples within the GPGP.

4.2. Submesoscale eddies and Buoyant Plastic Debris Characterization

This study provides a detailed characterization of floating plastic debris within the eastern North Pacific Ocean. From the results, the sea surface environment from all three regions, the outside, transition zone, and inside the GPGP, is dominated by 'H' type-plastics in numerical and mass concentration. Our results also demonstrate that Micro 1 is the leading size class distributed throughout all three regions within the anti-cyclonic submesoscale eddy (i.e. high SLA).

However, these observations could be explained due to windage or direct wind transport (Lebreton et al., 2018; Van Sebille et al., 2020). Direct wind transport effects protruding floating plastic debris which is exposed to the sea surface. There are two factors that influence windage,

(i) skin drag (i.e. the type of friction that is on the surface of the protruding floating plastic) and (ii) form drag (i.e. the type of pressure the wind applies to the surface of the protruding floating plastic) (Van Sebille et al., 2020). A large protruding floating plastic debris exposed to the wind will have a higher probability of being transported across the open ocean and onto other shores due to wind exposure. Conversely, a small heavier plastic, which is fully saturated at the sea surface, has a higher probability to be transported and accumulate within oceanic currents and gyre formations. A similar conclusion by a previous study was reached by objects with low or null windage coefficient captured within their trawls, which exhibited very little air drift when placed in sea water (Lebreton et al., 2018), while larger plastics, which have a higher windage drag had a higher likelihood of exiting the ocean 'garbage patch'. Despite the fact that Micro 1 and plastic 'H' type has the potential capacity to persist at the sea surface for a long residency time and accumulate and increase within both anti-cyclonic and cyclonic submesoscale eddies located from the outside moving into the GPGP, it is not a significant finding due to the oceanic processes (i.e. windage and surface currents), which can also influence the transport and accumulation of these specific characteristics observed.

4.3. Cyclonic Submesoscale Eddies within the Outside and Transition Zone into the GPGP

In regards to the outer and transition zone into the GPGP, the results show a trend depicting higher numerical and mass concentrations of floating plastic debris accumulating within a cyclonic submesoscale eddy when compared to an anticyclonic eddy (see Figure 4 and 6). These observations challenge the traditional cyclonic dispersal rotation characteristic. It also challenges the observation that anti-cyclonic eddies accumulate more floating plastic debris than cyclonic submesoscale eddies (Brach et al., 2018). However, these findings are consistent with recent research showing that floating plastic particles do accumulate within cyclonic vortices due to vortex stretching of the submesoscale vortices (D'Asaro et al, 2018). Another possible explanation that could be potentially causing surface convergence of floating plastic particles could depend on the Rossby number. The Rossby number, a dimensionless number describing fluid flow, is defined as the velocity (U) divided by the length (L) and Coriolis frequency (f). Therefore, a cyclonic

submesoscale with a smaller diameter (L) will signify a large Rossby number which generates strong centrifugal forces. Therefore, the cyclonic eddies have the potential to accumulate more floating plastic debris within its small but fast rotation. However, the results also demonstrate large ranges in numerical and mass concentrations between measurements taken across cyclonic submesoscale eddies. Major currents (i.e. California Current) and physical oceanic processes such as Langmuir circulation and internal tides can also influence the dispersal distribution of floating plastic accumulation (E van Sebille et al., 2020).

Figure 10 shows the predicted numerical concentrations from the oceanic transport model from Lebreton et al. (2018) plotted against the in-situ measured plastic particle corresponding to SLA categories. The comparison shows a disproportionate numerical distribution of the in-situ measurements taken from the low SLA category demonstrated within regions A (outside GPGP) and B (transition zone). The four samples extracted from the low SLA area from region A demonstrates a measurement that is approximately 2 orders of magnitude from the predicted fitted line. While the two samples extracted from the low SLA area from region B demonstrates a measurement that is approximately 3 orders of magnitude from the predicted fitted line. The sporadic distribution observed suggests an increase in heterogeneous spatial distribution of floating plastic debris within the cyclonic submesoscale eddies recorded within the outer and transitional zone into the GPGP. A hypothesis is that the outer and transitional zone are located closer to the continental shelf break, which generates internal tides and in turn generate internal waves, which can propagate for long distances (E van Sebille et al., 2020). Although these six low SLA outliers emerge from region A and B from the figure 10, the remaining in-situ data is well within one order of magnitude from the predicted estimations. Therefore, incorporated submesoscale forcing as an additional parameter is not necessary.

4.4. Anti-cyclonic Submesoscale Eddies Inside the GPGP

The anti-cyclonic submesoscale eddy analyzed inside of the GPGP indicated the highest numerical and mass concentration in comparison to the cyclonic submesoscale eddies recorded outside or within the transition zone. This is consistent with what has been found in the previous Brach et al

(2018) study. However, the spatial distribution pattern of floating plastic pollution observed, the outside, transition zone, and inside the GPGP increasing systematically, is in line with the general spatial distribution previously observed in the eastern North Pacific (Cozar et al., 2014; Eriksen et al., 2014; Lebreton et al., 2018). Therefore, the significantly higher concentrations observed within the anti-cyclonic submesoscale eddies could be due to the accumulation of floating plastic debris, which has already been collecting within this well-documented subtropical gyre. In addition, it is acknowledged that there are considerable discussions among researchers as to barotropic currents, fluid density that is only dependent on pressure, having an effect on microplastic transport and distribution in the open ocean. A recent model simulating the outcome of advection of microplastic particles with and without barotropic tidal currents concluded that the garbage patch regions are not affected by the tides (Sterl et al., 2020).

The results also demonstrate very large ranges in numerical and mass concentration measurements taken between and across anti-cyclonic submesoscale eddies. The geographical location (i.e. farther proximity from land mass) may decrease the amount of physical oceanic processes (i.e. major currents and internal tides) but the region remains susceptible to Langmuir circulation and stokes drift which are found ubiquitously throughout the open ocean (Van Sebille et al., 2020). Despite anti-cyclonic submesoscale eddies demonstrating large ranges of floating plastic accumulation and are composed of barotropic currents and vorticity formation dynamics, the general trend could potentially influence higher accumulations of numerical and mass concentrations of floating plastic debris within the North Pacific Gyre.

4.5. Limitations and Future Research

Throughout this research certain limitations were encountered due to the unfortunate repercussions and inconveniences encountered due to the COVID-19 global pandemic. The small sample size (n = 45) used to analyze the correlation between sub-mesoscale eddies and buoyant plastic distribution was the main limiting factor regarding this study. Another limiting factor is that this study was unable to compare cyclonic and anti-cyclonic submesoscale eddies within the parameters inside the GPGP due to the specific SLA parameter calculations derived from including

region A, B, and C together. Therefore, it would be beneficial to increase the sample size along with analyzing the difference in plastic accumulation and spatial distribution between anti-cyclonic and cyclonic submesoscale eddies solely within the GPGP region (Region C). Fortunately, daily satellite SLA records and Manta trawl metadata sets are readily available online. That way, future researchers can take the total SLA range within this particular area (i.e. inside the GPGP) and divide it into three equal intervals and categorize into low, medium, and high and observe the spatial distribution between each category. Additionally, and most importantly, the open ocean is highly influenced by not only sub-mesoscale dynamics, but a plethora of other oceanic processes that can highly influence the scales of spatial heterogeneity of buoyant plastic marine debris demonstrated throughout this study. Therefore, the extent to which it is possible to track a hotspot within a highly variable and dynamic eddy is unknown. In order to better understand the spatial accumulation patterns, it would be beneficial for future research to conduct a more detailed floating plastic debris sampling campaign throughout the genesis, spatial trajectory over time, and decay of an eddy formation within the GPGP. This information is important as future offshore ocean cleanup efforts could use these oceanic processes as a natural accumulating instrument to alleviate the dynamic locations of floating plastic accumulation hotspots within the GPGP.

4.6. Mitigation Strategies

As various clean up organizations continue to work towards removing floating plastic debris throughout the subtropical gyres, the results of this study show higher concentrations of hard ('H') type plastics with the size range between Micro 1 (0.05 cm to 0.15 cm) to Meso 2 (1.5 cm to 5 cm) accumulating within the inside of the Great Pacific Garbage Patch. Therefore, in order to be more efficient regarding the removal of floating plastic particles, future mechanisms or machinery should incorporate trapping and sustaining particular plastic debris exhibiting these characteristics.

5. Conclusion

This research aimed to identify how anti-cyclonic and cyclonic submesoscale eddies are impacting the distribution of floating plastic debris within the eastern North Pacific Ocean. Based on numerical (#/km^2) and mass (kg/km^2) concentrations of floating plastic debris according to Sea Level Anomaly categories (SLA, m), while the trend is observed that anti-cyclonic eddies demonstrate higher concentrations of floating plastic debris inside the Great Pacific Garbage Patch (GPGP) than outside or along the transition zone into the GPGP, these findings are not significant. The results indicate large variations in numerical and mass concentrations, which indicate large spatial heterogeneous patterns within both, cyclonic and anti-cyclonic submesoscale eddies. Despite these trends, when comparing in-situ measurements to estimated dispersal model predictions, in-situ measurements corresponding to cyclonic and anti-cyclonic parameters do not indicate a significant difference. Based on the different plastic types and plastic size classes in numerical (#/km^2) and mass (kg/km^2) concentrations of floating plastic debris according to SLA, a trend of 'H' type (i.e. hard plastic) and Micro 1 (0.05 cm – 0.15 cm) class size is represented as the largest fraction of plastic assemblage for anti-cyclonic submesoscale eddies. Despite trends observed, there are other oceanic processes occurring in these regions that were not considered in the scope of this project. In the future, a more complete picture could be determined based on research that includes stokes drift and Langmuir circulation. The inclusion of these other processes with an increased sampling size is recommended for future projects in this area.

6. References

Andrady, A. L. (2011). Microplastics in the marine environment. *Marine pollution bulletin*, *62*(8), 1596-1605.

Brach, L., Deixonne, P., Bernard, M. F., Durand, E., Desjean, M. C., Perez, E., ... & ter Halle, A. (2018). Anticyclonic eddies increase accumulation of microplastic in the North Atlantic subtropical gyre. *Marine pollution bulletin*, *126*, 191-196.

Chelton, D. B., Gaube, P., Schlax, M. G., Early, J. J., & Samelson, R. M. (2011). The influence of nonlinear mesoscale eddies on near-surface oceanic chlorophyll. *Science*, *334*(6054), 328-332.

Cheng, Y. H., Ho, C. R., Zheng, Q., & Kuo, N. J. (2014). Statistical characteristics of mesoscale eddies in the North Pacific derived from satellite altimetry. *Remote Sensing*, *6*(6), 5164-5183.

Cózar, A., Echevarría, F., González-Gordillo, J. I., Irigoien, X., Úbeda, B., Hernández-León, S., ... & Fernández-de-Puelles, M. L. (2014). Plastic debris in the open ocean. *Proceedings of the National Academy of Sciences*, *111*(28), 10239-10244.

D'Asaro, E. A., Shcherbina, A. Y., Klymak, J. M., Molemaker, J., Novelli, G., Guigand, C. M., ... & Huntley, H. S. (2018). Ocean convergence and the dispersion of flotsam. *Proceedings of the National Academy of Sciences*, *115*(6), 1162-1167.

Egger, M., Sulu-Gambari, F., and Lebreton, L. (2020). First evidence of plastic fallout from the Great Pacific Garbage Patch. *Sci. Rep.*, 1–10. doi:10.1038/s41598-020-64465-8.

Eriksen, M., Lebreton, L. C., Carson, H. S., Thiel, M., Moore, C. J., Borerro, J. C., ... & Reisser, J. (2014). Plastic pollution in the world's oceans: more than 5 trillion plastic pieces weighing over 250,000 tons afloat at sea. *PloS one*, *9*(12), e111913.

Fu, L. L., Chelton, D. B., Le Traon, P. Y., & Morrow, R. (2010). Eddy dynamics from satellite altimetry. *Oceanography*, *23*(4), 14-25.

Geyer, R., Jambeck, J. R., & Law, K. L. (2017). Production, use, and fate of all plastics ever made. *Science advances*, *3*(7), e1700782.

Goldstein, M. C., Titmus, A. J., & Ford, M. (2013). Scales of spatial heterogeneity of plastic marine debris in the northeast Pacific Ocean. *PloS one*, *8*(11), e80020.

Hidalgo-Ruz, V., Gutow, L., Thompson, R. C., and Thiel, M. (2012). Microplastics in the marine

environment: A review of the methods used for identification and quantification. *Environ. Sci. Technol.* 46, 3060–3075. doi:10.1021/es2031505.

Kukulka, T., Proskurowski, G., Morét-Ferguson, S., Meyer, D. W., & Law, K. L. (2012). The effect of wind mixing on the vertical distribution of buoyant plastic debris. *Geophysical Research Letters*, *39*(7).

Law, K. L. (2017). Plastics in the marine environment. *Annual review of marine science*, *9*, 205-229.

Lebreton, L. C. M., Van Der Zwet, J., Damsteeg, J. W., Slat, B., Andrady, A., and Reisser, J. (2017). River plastic emissions to the world's oceans. *Nat. Commun.* 8, 1–10. doi:10.1038/ncomms15611.

Lebreton, L., Slat, B., Ferrari, F., Sainte-Rose, B., Aitken, J., Marthouse, R., ... & Noble, K. (2018). Evidence that the Great Pacific Garbage Patch is rapidly accumulating plastic. *Scientific reports*, *8*(1), 1-15.

Lebreton, L., Egger, M., & Slat, B. (2019). A global mass budget for positively buoyant macroplastic debris in the ocean. *Scientific reports*, *9*(1), 1-10.

PlasticsEurope, & EPRO. (2018). Plastics – the Facts 2018 An analysis of european plastics production, demand and waste data. In *Plastics – the Facts 2018*.

Ryan, P. G., Moore, C. J., van Franeker, J. A., & Moloney, C. L. (2009). Monitoring the abundance of plastic debris in the marine environment. *Philosophical Transactions of the Royal Society B: Biological Sciences*, *364*(1526), 1999-2012.

Sigler, M. (2014). The effects of plastic pollution on aquatic wildlife: current situations and future solutions. *Water, Air, & Soil Pollution*, *225*(11), 2184.

Sterl, M. F., Delandmeter, P., & van Sebille, E. (2020). Influence of barotropic tidal currents on transport and accumulation of floating microplastics in the global open ocean. *Journal of Geophysical Research: Oceans*, *125*(2), e2019JC015583.

UNEP (2016). Marine plastic debris & microplastics - Global lessons and research to inspire action and guide policy change.

Van Sebille, E. (2015). The oceans' accumulating plastic garbage. Phys. Today 68 (2), 60-61.

Van Sebille, E., Aliani, S., Law, K. L., Maximenko, N., Alsina, J. M., Bagaev, A., ... & Delandmeter, P. (2020). The physical oceanography of the transport of floating marine debris. *Environmental Research Letters*, *15*(2), 023003.

7. Acknowledgments

I would like to thank from the bottom of my heart my supervisor, Matthias Egger, for his guidance and beneficial feedback throughout the research process, including redirecting the project as a result of COVID-19. I would also like to thank, Dr. Thilo Behrends, for dedicating his time to reviewing my thesis project and also being incredibly supportive through the personal hardships I endured throughout the duration of this project. Finally, I would like to dedicate my love, passion, and contribution to mitigate plastic pollution from our precious marine environment to my loving Abuelita, Maria Amparo Carranza Saenz, who I lost during the global pandemic.